Future Changes in Seasonality in East Africa from Regional Simulations with Explicit and Parameterized Convection

CAROLINE M. WAINWRIGHT,[a,b] JOHN H. MARSHAM,[c] DAVID P. ROWELL,[d] DECLAN L. FINNEY,[c] AND EMILY BLACK[a,b]

[a] *Department of Meteorology, University of Reading, Reading, United Kingdom*
[b] *National Centre for Atmospheric Science, Reading, United Kingdom*
[c] *School of Earth and Environment, University of Leeds, Leeds, United Kingdom*
[d] *Met Office Hadley Centre, Exeter, United Kingdom*

(Manuscript received 11 June 2020, in final form 1 October 2020)

ABSTRACT: The East African precipitation seasonal cycle is of significant societal importance, and yet the current generation of coupled global climate models fails to correctly capture this seasonality. The use of convective parameterization schemes is a known source of precipitation bias in such models. Recently, a high-resolution regional model was used to produce the first pan-African climate change simulation that explicitly models convection. Here, this is compared with a corresponding parameterized-convection simulation to explore the effect of the parameterization on representation of East Africa precipitation seasonality. Both models capture current seasonality, although an overestimate in September–October in the parameterized simulation leads to an early bias in the onset of the boreal autumn short rains, associated with higher convective instability and near-surface moist static energy. This bias is removed in the explicit model. Under future climate change both models show the short rains getting later and wetter. For the boreal spring long rains, the explicit convection simulation shows the onset advancing but the parameterized simulation shows little change. Over Uganda and western Kenya both simulations show rainfall increases in the January–February dry season and large increases in boreal summer and autumn rainfall, particularly in the explicit convection model, changing the shape of the seasonal cycle, with potential for pronounced socioeconomic impacts. Interannual variability is similar in both models. Results imply that parameterization of convection may be a source of uncertainty for projections of changes in seasonal timing from global models and that potentially impactful changes in seasonality should be highlighted to users.

KEYWORDS: Africa; Precipitation; Climate change; Convective parameterization; Seasonal cycle

1. Introduction

Recent extreme wet seasons over East Africa have had a range of serious socioeconomic consequences; the successive failure of the 2018 short rains (October–December) and the 2019 long rains (March–May) led to drought and decreased food security in Kenya in mid-2019. Conversely, above average rainfall was experienced during the 2018 long rains (Kilavi et al. 2018; Finney et al. 2020b) and 2019 short rains, with many locations receiving more than double the climatological rainfall during October–December 2019 (Wainwright et al. 2020). The anomalously wet short rains in 2019 led to flooding and landslides, with an estimated 2.8 million people affected across East Africa. This was followed by a wet 2020 long rains leading to a large and rapid rise in the level of Lake Victoria in early 2020 to record-breaking levels, with more floods and people displaced.

Precipitation seasonality is of significant socioeconomic importance for East Africa, as it impacts agricultural productivity and food security; late onset and drier than average wet seasons lead to crop failure and decreased food security. The timing of onset is particularly important for the initial stages of crop development. Conversely, very wet seasons can adversely affect crops such as tomatoes. Seasonal rainfall also affects replenishment of water in reservoirs for hydroelectric energy generation, and the prevalence of vectors that transmit diseases such as malaria. Recent declines in the long rains, due to later onset and earlier cessation of the season, have had detrimental consequences over East Africa (Wainwright et al. 2019). Understanding and preparing for possible changes in the timing and amount of seasonal rainfall is crucial for successful adaptation to future climate change.

The use of climate model projections of future climate change over East Africa is often perceived as problematic given that coupled climate models fail to correctly represent the present-day seasonal cycle, with the long rains underestimated and too late, and the short rains overestimated

Denotes content that is immediately available upon publication as open access.

Supplemental information related to this paper is available at the Journals Online website: https://doi.org/10.1175/JCLI-D-20-0450.s1.

Corresponding author: Caroline M. Wainwright, c.wainwright@reading.ac.uk

DOI: 10.1175/JCLI-D-20-0450.1

(Tierney et al. 2015; Yang et al. 2015b; Dunning et al. 2017; Ongoma et al. 2019; Ayugi et al. 2020; Mumo and Yu 2020). Yang et al. (2015b) found that atmosphere-only models do reproduce the biannual seasonal cycle but overestimate the rainfall in all months except April and May. This overestimate in October–December (short rains) is such that the short rains are almost comparable with the long rains (Yang et al. 2015b). This is larger in the coupled simulations, which show more rainfall in the short rains than the long rains (Tierney et al. 2015), opposite to that observed in reality. The role of these biases on future projections is unknown; notably for seasonal prediction the bias is largest during the short rains, but the skill is also highest for the short rains (Walker et al. 2019).

The atmosphere-only and coupled climate model simulations produced as part of phase 5 of the Coupled Model Intercomparison Project (CMIP5; Taylor et al. 2012) and the Coordinated Regional Climate Downscaling Experiment (CORDEX; Giorgi et al. 2009) all use parameterization schemes to represent the average effects of convection. The parameterization of convection in climate models is a known source of model error, resulting in biases in timing of the diurnal cycle of precipitation and biases in rainfall amount, with an underestimation of hourly precipitation intensities and too many low-precipitation events on daily time scales (Prein et al. 2015). In the tropics, parameterization of convection can mean models are unable to correctly represent organized propagating systems (Kendon et al. 2019; Crook et al. 2019), which are a key part of some tropical climates (Vellinga et al. 2016). Biases in the cloud and rainfall model fields, resulting from the use of parameterized convection, interact and influence other fields, including radiation, and can lead to a range of consequences, including upscale effects on larger scales, such as monsoons (Marsham et al. 2013; Taylor et al. 2013; Birch et al. 2014a; Willetts et al. 2017; Finney et al. 2019). Differences in the simulated strength of entrainment into convection have also been linked to the uncertainty in climate sensitivity (Sherwood et al. 2014).

Models with high spatial resolution (<4 km) can represent convection explicitly without the need for a convection scheme; such models are termed ''convection-permitting'' (Prein et al. 2015). Convection-permitting models (CPMs) are used operationally for forecasting across the world and have led to a large improvement in the skill of short-range precipitation forecasts (Clark et al. 2016). CPMs have been found to better represent extreme precipitation on hourly time scales and the diurnal cycle of precipitation, lead to improved representation of precipitation structures (Prein et al. 2015), and resolve mesoscale convective organization (Stratton et al. 2018). However, the high computational demand of CPMs limits the length of simulations available.

As part of the Future Climate for Africa (FCFA) Improving Model Processes for African Climate (IMPALA) project, two 10-yr simulations of the Met Office Unified Model (MetUM) were performed at convection-permitting (4.5 km) resolution for a pan-Africa domain (CP4A; Stratton et al. 2018; Kendon et al. 2019). One simulation is for the present climate (1997–2007) and one is for an idealized future climate (circa 2100 under a high-emissions scenario). This is the first time that climate-length convection-permitting simulations have been completed for the African continent (Stratton et al. 2018; Kendon et al. 2019). Two comparable simulations were also completed at 25-km resolution with parameterized convection (P25). By comparing these simulations, the impact of convective parameterization on African climate variability and climate change can be explored. While previous studies have examined the impact of CPMs on short time scales over Africa, these simulations enable us to examine the impact of CPMs on longer time scales.

Stratton et al. (2018) analyzed the first five years of the present-climate CP4A (hereinafter simply CP4) simulations and found notable improvements in the representation of boreal summer rainfall compared with P25, with a reduction in the persistent dry bias in West Africa, found in many versions of the MetUM (Williams et al. 2015; Walters et al. 2017). Berthou et al. (2019b) found that CP4 gave an improved representation of the mature phase of the West African monsoon and better distribution of precipitation rates, resulting in better representation of wet and dry spells. They also found an improvement in the diurnal cycle of rainfall, a well-documented expected improvement from using CPMs (Prein et al. 2015). Kendon et al. (2019) (see also Berthou et al. 2019a; Finney et al. 2020a; Fitzpatrick et al. 2020) explored the climate change signal in CP4 and P25, and found that the convection-permitting model contained increases in dry spell length during the wet season, not found in P25. CP4 also exhibited greater increases in extreme 3-hourly precipitation than P25, leading to the conclusion that projected changes in both wet and dry extremes over Africa may be more severe than previous results from parameterized convection models indicated.

The main improvements of using CPMs are found when deep convection is a dominant process and in regions with strong spatial heterogeneities (Prein et al. 2015). As is typical of the tropics, convective systems contribute most to annual rainfall totals over East Africa, and orography ranges from coastal regions adjacent to the Indian Ocean to mountainous regions within the East African Rift Valley, with elevations greater than 4000 m (Dinku et al. 2007). Thus, over East Africa it would be expected that the use of CPMs would yield substantial improvements. When examining short-range forecasts over East Africa, Woodhams et al. (2018) found that a convection-permitting model had the greatest skill improvement relative to a global model over land in East Africa.

Finney et al. (2019) provided an evaluation of rainfall in the present-day CP4 and P25 simulations, with a specific focus on the Lake Victoria Basin. They showed an improvement in contribution of extreme rain rates to total rainfall and the diurnal rainfall cycle in CP4 compared to P25. Finney et al. (2019) carried out a simple seasonal analysis (based on month groupings) of total rainfall. In this regard there were no substantial improvements upon the P25 simulation; however, the onset and cessation of the rainy seasons were not considered and the effect of differences in season timing was not accounted for in analysis of the variability and changes. Similar results were found on the broader African continent scale by Kendon et al. (2019), but again the onset and cessation dates were not analyzed. In the future climate change simulations,

Finney et al. (2020a) find that P25 fails to capture the widespread increases in rainfall extremes shown by the convection-permitting simulation across East Africa. Furthermore, although the P25 simulation captures the changes in the sea-breeze circulation under future climate change found in the CP4 simulation, it does not capture the rainfall response to these changes. Overall, these studies suggest important improvements from using convection-permitting simulations over East Africa, and differences in the future projections (Finney et al. 2020a).

High dependence upon rain-fed agriculture makes the seasonal rainfall across East Africa of significant societal importance; recent declines in the long rains, due to shorter seasons, have had adverse impacts on food security (Rowell et al. 2015; Wainwright et al. 2019). It is therefore important to understand how wet seasons may change under future climate change, but current model limitations, including the poor model representation of seasonality in both atmosphere-only and coupled CMIP5 models (Yang et al. 2015b), may limit the use of future projections of seasonality. Furthermore, the apparent discrepancy between recent observed declines in the long rains and projected future increases in the long rains limits the use of climate information in adaptation planning (Rowell et al. 2015; Wainwright et al. 2019; Ongoma et al. 2018; Dosio et al. 2019; Gebrechorkos et al. 2019). Dunning et al. (2018) produced projections of changes in seasonal timing and rainfall totals under future climate change over East Africa using CMIP5 models; they found the short rains are projected to start and end later, with an increase in short rains rainfall. The long rains are projected to end earlier, but there was no multimodel consensus on changes in long rains rainfall totals.

Given the wider-scale improvements in the representation of East African climate from using convection-permitting models (Finney et al. 2019; Kendon et al. 2019), and the high socioeconomic importance of precipitation seasonality, here we aim to explore the representation of precipitation seasonality over East Africa in both the CP4 and P25 simulations. For the future use of these simulations, and to inform future simulation design, it is important to understand how models capture the seasonality, changing seasonality under future climate change, and the interannual variability when models are run in an atmosphere-only configuration, with shared sea surface temperatures and atmospheric boundary conditions. First we explore the interannual variability in both simulations; interannual variability is often understood in terms of teleconnections, whereby a remote driver influences local rainfall over land, via an atmospheric pathway. In simulations such as those used in this study that remote driver will generally be external to the regional model, but the regional model can affect the local response of convection and it is known that in the tropics that explicit convection can have upscale effects to mean state.

In their studies Finney et al. (2019) and Kendon et al. (2019) take a simple approach to seasonality and focus on the mean state and extremes. Here we extend this by calculating onset and cessation dates for both East African wet seasons and comparing with satellite-based precipitation datasets to determine whether the use of convective parameterization adversely affects the representation of seasonality in the model. Onset and cessation dates are compared for the present- and future-climate simulations, to determine if the projections of changing seasonality under future climate change are consistent with the CMIP5 projections, and whether they are affected by the representation of convection. To further explore the identified differences between CP4 and P25, the differences and changes in the annual cycles of moist static energy and convective instability are presented. Finally, changes in the shape of the seasonal cycle are explored, with the high horizontal resolution in CP4 and P25 enabling us to explore changing seasonality over small regions with distinct seasonal regimes.

2. Models, methods, and data

a. Model simulations

We analyze four model simulations produced using regional climate models based on the Met Office Unified Model (MetUM) over an African domain (45°S–39°N, 25°W–56°E). All simulations are run for 10 years and 2 months (starting on 1 January); to have full calendar years for analysis, here just the first 10 years are used. The key results are not for January or February, so it was decided that using the first two months would have minimal impact. Two simulations are run for a present climate (January 1997–February 2007) and two are run for an idealized future climate. For both the present and future climates, one simulation is run with explicit convection (CP4) and one with parameterized convection (P25). Here we use daily precipitation data, and monthly temperature (1.5 m and 700 hPa), specific humidity (1.5 m), and geopotential height (700 hPa). Full details of the model specifications and setup can be found in Stratton et al. (2018) and Kendon et al. (2019); a brief overview is given here.

1) Global model, common setup, and driving data

Both the CP4 and P25 models are one-way nested within a MetUM Global Atmosphere/Land, version 7.0 (GA7/GL7; Walters et al. 2019), simulation run at N512 horizontal resolution (~26 km in latitude by 39 km in longitude over Africa), with 85 levels in the vertical direction and an upper boundary at 85 km. The global model provides lateral boundary conditions to the regional model and includes convective parameterization. The Joint U.K. Land Environment Simulator (JULES) land surface scheme is used to calculate fluxes of energy, water, and momentum into the atmosphere from the land surface. Sandy soils are used uniformly across the domain to avoid differences in precipitation due to unrealistic small-scale variations in soil type (De Kauwe et al. 2013).

For the two present climate simulations, the global model is driven using analyses of observed sea surface temperature (SST) over 1997–2007 (Reynolds et al. 2007). For the future climate simulations, SSTs are the sum of Reynolds SST analyses over 1997–2007 and the climatological average SST change from 1975–2005 to 2085–2115 from a HadGEM2-ES simulation, using the RCP8.5 scenario (high emissions; van

Vuuren et al. 2011). SST changes were calculated for each month, then interpolated both spatially and temporally, and added to the daily varying SST analysis forcing data (Reynolds et al. 2007) on the various model grids. The increase in SST corresponds to a global mean SST increase of just under 4 K and a global mean 1.5-m air temperature change of 5.2 K. This approach means that the present-climate and future-climate (and CP4 and P25) simulations share much of the same SST variability. For the present-climate simulation greenhouse gas (GHG) mass mixing ratios vary annually, with CO_2 varying from $5.516\,79 \times 10^{-4}\,kg\,kg^{-1}$ for 1997 to $5.814\,88 \times 10^{-4}\,kg\,kg^{-1}$ for 2006. For the future-climate simulation, GHG values were taken from the RCP8.5 scenario for 2100 (Kendon et al. 2019). The same aerosol and ozone climatologies are used in both present- and future-climate simulations.

2) Convection-permitting model (CP4)

The CP4 regional model is based upon the Met Office UKV regional model, which is used to produce weather forecasts for the United Kingdom (Stratton et al. 2018). Importantly, it does not include convective parameterization, and depends on model dynamics to explicitly represent convective processes. It covers the entirety of continental Africa, with horizontal grid spacing ranging from 3.2 km at 45°S to 4.5 km at 0°S. The horizontal resolution was chosen to balance the domain size and computational cost; thus, while it will partially resolve deep convection it will not resolve smaller-scale congestus or shallow convection (Stratton et al. 2018). Orography is applied at the regional model's raw resolution; thus, this is better resolved by the CP4 model than the P25 model. The CP4 regional model has 80 levels in the vertical direction with the model top at 38.5 km; it has more levels in the upper troposphere than the UKV in order to better resolve convection and the tropical troposphere. Moisture conservation schemes are employed in this model (and the global driving model); in the CP4 model this has the effect of reducing the mean precipitation values everywhere, bringing them closer to observations, and reducing the frequency of very high unrealistic precipitation rates (Stratton et al. 2018). For all analysis in this study, the CP4 data have been regridded to the N512 horizontal grid (first-order conservative remapping).

3) Parameterized convection model (P25)

The P25 regional model has the same physics configuration as the global model (GA7/GL7), including convective parameterization. It is run at N512 resolution and has 63 levels in the vertical direction with a model lid at 41 km. The P25 regional model has the same domain, land surface, and aerosol climatologies as CP4. Unlike CP4 and the global driving model, P25 does not include moisture conservation. There are also some differences in the boundary layer and cloud schemes [as described by Stratton et al. (2018)]. However, the explicit convection and higher resolution are expected to dominate the differences in seasonality. Indeed, Berthou et al. (2019b) compared their results with results from Cascade project studies (Pearson et al. 2010, 2014; Birch et al. 2014a), where they did not have differences in the cloud scheme, and found them to be similar, and thus concluded that majority of differences between CP4 and P25 are due to the representation of convection and resolution.

b. Rainfall observations

Because of the limited availability of rain gauge observations over East Africa, two satellite-based precipitation datasets are used as rainfall observations. The Tropical Rainfall Measuring Mission (TRMM) Multisatellite Precipitation Analysis 3B42, version 7, uses a combination of thermal infrared imagery, visible imagery, passive microwave imagery, radar, and rain gauge observations to produce 3-hourly precipitation estimates, and is available from 1998; here we have used daily rainfall estimates for 1998–2007 (Huffman et al. 2007). TAMSAT (Tropical Applications of Meteorology using Satellite data and ground-based observations) rainfall estimates were also used for comparison; estimates are available from 1983, and therefore it covers the entire CP4/P25 simulation period (Maidment et al. 2017). Because they cover the same period, TAMSAT, version 3 (TAMSATv3), data are used for statistical tests. Thermal infrared imagery, calibrated against observations from rain gauges, is used to produce daily rainfall estimates. TAMSATv3 daily rainfall data were used for 1997–2006. Both rainfall estimates have been regridded to the N512 grid (first-order conservative remapping).

c. Onset/cessation

To examine the representation of precipitation seasonality in the CP4 and P25 simulations, we quantify the seasonal cycle by calculating onset and cessation dates for one/two annual wet seasons. The methodology of anomalous accumulation is used to calculate onset and cessation dates; it is based on the method of Liebmann et al. (2012) and is fully described in Dunning et al. (2016). A brief overview is given here.

The first step is to determine which regions have one wet season per year (annual regime) and which regions have two wet seasons per year (biannual regime). Harmonic analysis is used to categorize annual and biannual seasonal regimes; at each grid point the ratio of the amplitude of the second harmonic to the amplitude of the first harmonic was computed. If the ratio is greater than 1, then the amplitude of the second harmonic is greater, and the grid point is classified as having a biannual seasonal regime. If the ratio is less than 1 then the grid point classified as an annual seasonal regime.

Onset and cessation dates were computed using the method based on cumulative rainfall anomalies (Liebmann et al. 2012; Dunning et al. 2016). This method works by identifying minima and maxima in the cumulative daily rainfall anomaly. The periods of the year when the wet seasons occur on average are found by identifying minima and maxima in the climatological cumulative daily rainfall anomaly; one season is identified for annual regimes and two seasons are identified for biannual regimes. These periods are termed the "climatological wet seasons." For each year and season, the period from 20 or 50 days (for the biannual and annual regimes, respectively; see Dunning et al. 2016) before the start of the climatological wet season to 20 or 50 days (again for the biannual and annual regimes, respectively) after the end of the climatological wet season is extracted, and the cumulative daily rainfall anomaly is calculated for this period. The minima in the cumulative daily rainfall anomaly are defined as the onsets, and the maxima (after the minima) are defined as the cessations.

A second method for determining onset dates was also proposed by Liebmann et al. (2012) based on the cumulative daily rainfall anomaly; in this method, for each day within the onset search

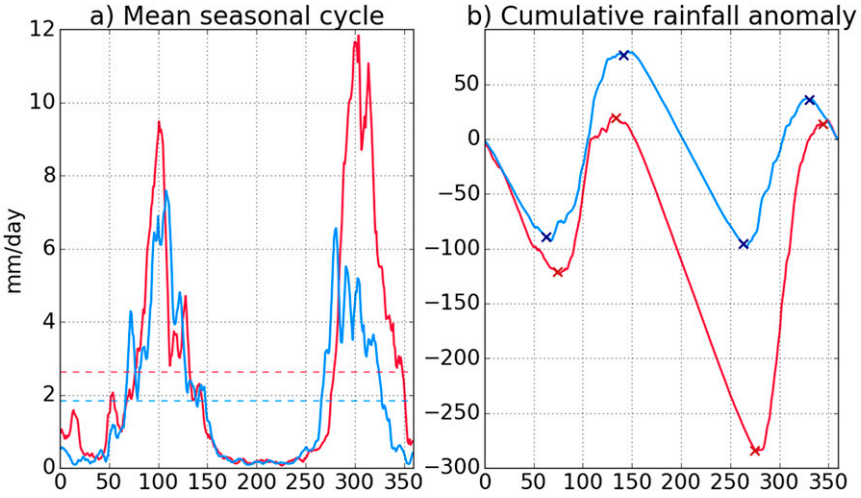

FIG. 1. This figure demonstrates the need to use present daily mean rainfall when computing future onset and cessation dates: (a) two example seasonal cycles (solid lines) and daily mean rainfall (dashed lines) (blue is for present, and red is for future), and (b) the cumulative daily rainfall anomaly for the same seasonal cycles; crosses mark the minima and maxima.

interval (from 20 or 50 days prior to the start of the climatological wet season to 20 or 50 days after the end of the climatological wet season), the number of days until the cumulative daily rainfall anomaly dips below the value on that reference day is counted. The day with the largest count is defined as the onset. Throughout this analysis both methodologies have been used to ensure robustness; results were consistent for both methodologies and are only shown for the first methodology (minima/maxima).

FUTURE CHANGES

Both methods used for calculating onset/cessation depend on the "cumulative daily rainfall anomaly," a quantity calculated by subtracting the annual mean daily rainfall from the daily rainfall, and then summing these anomalies. Both methods work by looking for minimum values in this quantity. Thus the onset and cessation are affected by the value of the mean daily rainfall.

Future climate projections from CMIP5 exhibit a greater increase in rainfall totals during short rains when compared with the long rains (Rowell et al. 2015; Dunning et al. 2018). Figure 1a shows an example; the red line (for the future) shows a large increase in the short rains, while there is only a small increase in the long rains. This leads to an increase in the daily mean rainfall (red dotted line versus blue dotted line).

This change in the daily mean rainfall results in a change of sign of the rainfall anomaly at the beginning and end of the long rains; rainfall at the beginning and end of the season that previously gave a positive anomaly now gives a negative anomaly. Thus, the minima occur later and the maxima occur earlier (Fig. 1b); the onset has gotten later and cessation has gotten earlier despite little change in rainfall in the long rains.

This may be a problem when analyzing future changes: onset/cessation dates for the long rains may alter due to large increases in the amount of rainfall occurring during the short rains. To account for this, in this analysis the mean daily rainfall from the present climate simulation (at each grid point) is used to compute future onset and cessation dates. While this may also have some limitations, a consistent algorithm is applied to all model simulations and observations, so onset and cessation dates, and projections, are comparable, and effects of explicit convection can be identified.

d. *Moist static energy*

Yang et al. (2015a) analyzed the convective instability over East Africa and proposed that the precipitation annual cycle over East Africa is modulated by the near-surface moist static energy (MSE). Furthermore, when investigating the bias in the East African precipitation annual cycle in coupled models, as compared with atmosphere-only models, Yang et al. (2015b) found that the rainfall bias can be explained by the bias in convective instability, which is dominated by the bias in the near-surface moist static energy. These metrics are also computed here to explore the differences between the CP4 and P25 simulations. MSE is defined as

$$h = c_p T + Lq + gz, \tag{1}$$

where c_p is the specific heat capacity at constant pressure, T is the temperature (K), L is the latent heat of evaporation, q is the specific humidity, g is the gravity acceleration, and z is the height above the surface. The conditional instability can be defined as the difference between the surface MSE (h_s) and the saturated MSE at 700 hPa ($h^*_{700\text{hPa}}$), as defined in Yang et al. (2015a). Monthly 1.5-m temperature and specific humidity were used to calculate surface MSE. Monthly 700-hPa temperature and geopotential height were used to compute saturated MSE at 700 hPa; however, pressure-level diagnostics were not enabled for the first 6 months of the 4-km present-climate simulation, and therefore $h^*_{700\text{hPa}}$ is not calculated for January–June 1997 for this simulation.

e. *Statistical tests*

Because the P25 and CP4 simulations have the same boundary conditions, and are driven by the same global model simulation, it

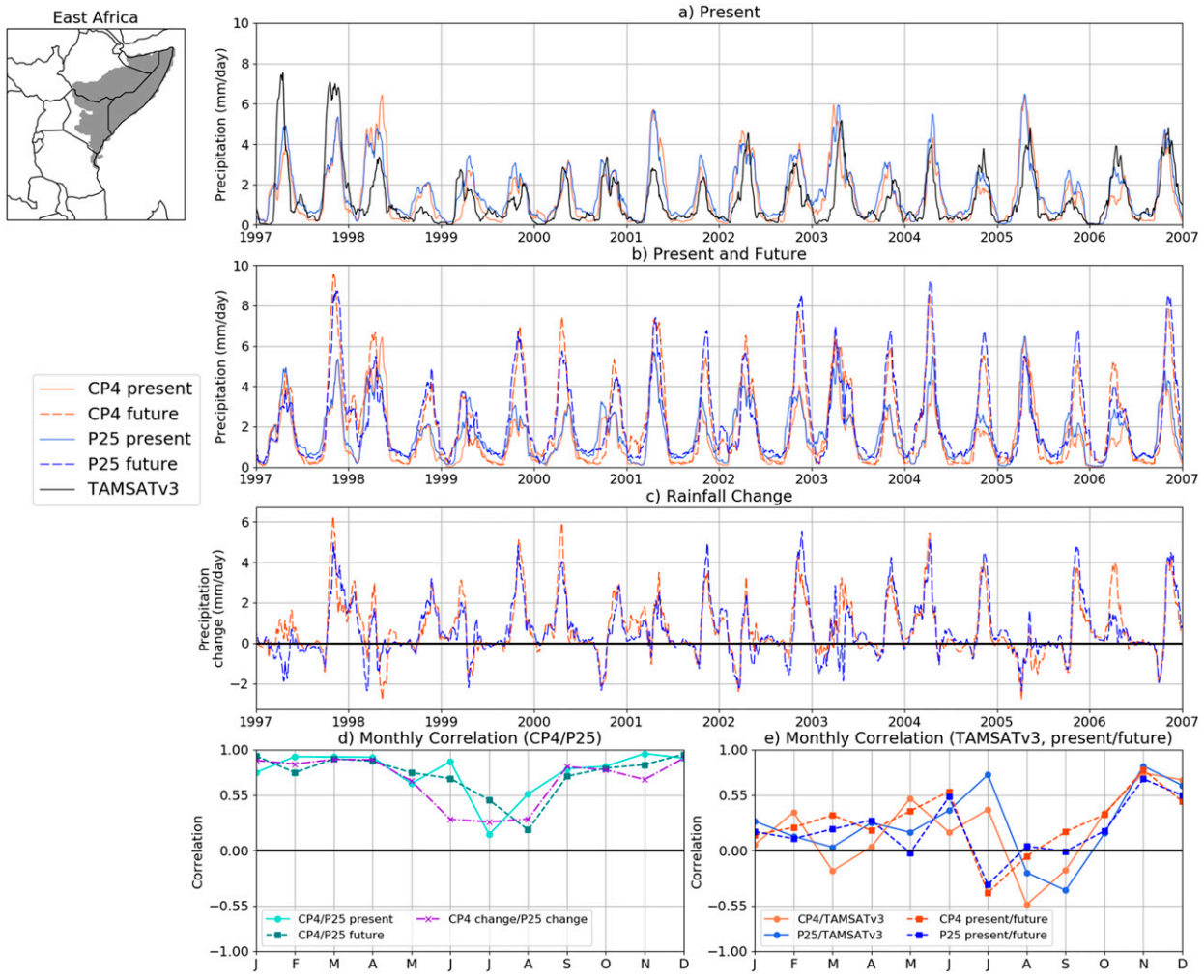

FIG. 2. Time series of rainfall over East Africa (the region shown on the inset map): (a) Observed rainfall (TAMSATv3) and rainfall from CP4 and P25 present-climate simulation for 1997–2006. (b) Rainfall from CP4 and P25 present- and future-climate simulations. (c) Future − present difference for CP4 and P25. All time series were smoothed using a 31-day moving average. (d),(e) Monthly correlations between the time series; different colors and lines indicate different pairings of model and observation time series. The value on the *y* axis is the Pearson correlation coefficient. Correlation coefficients greater than 0.55 indicate statistical significance at the 90% confidence interval.

would be incorrect to assume independence when comparing the P25 and CP4 simulations. Therefore, we cannot use a *t* test to establish the statistical significance of these differences (von Storch and Zwiers 1999, and elsewhere). Here, the paired difference test has been used; this works by computing the difference fields and testing the null hypothesis that the mean difference is 0. Full details can be found in von Storch and Zwiers (1999). All tests are done using a 90% confidence level.

3. Results

a. Interannual variability

The overall aim of this paper is to explore the effects of convective parameterization on the representation of precipitation seasonality over East Africa under present and future climates; this will be achieved by comparing the CP4 and P25 simulations described in section 2. First, it is helpful to explore the role of remote versus internal drivers and the sensitivity of this to convective representation (CP4 vs P25). Understanding the drivers of interannual variability (utilizing the fact that these two simulations have identically varying boundary conditions) is an important precursor for both understanding and testing the sensitivity of the 10-yr mean seasonality to convective representation. Information on the sensitivity of interannual variability to local versus remote drivers, and to a model's representation of convection, is also important in its own right for further improving its modeling and prediction. Here we examine the interannual variability in both the present- and future-climate simulations and compare CP4 with P25, and both models with rainfall observations.

Figure 2 shows the precipitation time series from the CP4 and P25 simulations (and TAMSATv3 observations) for 1997–2006 averaged over an East Africa region. This region is used to define the part of East Africa that experiences a biannual

rainfall regime and is used throughout the paper; it is the same region as is used in Wainwright et al. (2019) and is similar to the region used in Rowell et al. (2015). Correlations were computed for each month; the results are shown in Figs. 2d and 2e. Figure 2a demonstrates that the interannual variability is very similar in the CP4 and P25 simulations; monthly correlations between the two (CP4 and P25) present-climate simulations are generally high, with values for wet season months (March, April, May, October, November, and December) ranging between 0.66 and 0.96 (all significant at 90% confidence interval; Fig. 2d). Correlations are lower in the boreal summer dry season months (especially July and August), but above 0.75 in January and February. These high CP4/P25 correlation values demonstrate that the interannual variability is primarily controlled from the SSTs and atmospheric boundary conditions, and only marginally influenced by the representation of convection and factors within the regional domain. This is true of both wet seasons; while we would expect the interannual variability in the short rains to be driven by larger-scale factors, from outside the regional domain [such as El Niño–Southern Oscillation (ENSO) and the Indian Ocean dipole (IOD); Nicholson 2017], these results confirm that in these simulations the interannual variability in the long rains is also largely controlled by the combination of the SSTs and atmospheric boundary conditions (known to be important for the long rains; Vellinga and Milton 2018). Lower correlations during the boreal summer months may be related to low rain rates or the role of local processes. Overall, this confirms that compared with comparing two coupled global models for 10 years, the role of internal variability in affecting the difference in mean state between the two models is massively reduced, as the interannual variability is so constrained by SSTs and boundary conditions.

When comparing the two (CP4 and P25) future-climate simulations, monthly correlations for wet season months range between 0.77 and 0.95 (significant at 90% confidence interval), again demonstrating the similarity in the interannual variability (Figs. 2b,d). Monthly correlations for the future-present change in CP4 and P25 are also high in wet season months, with values ranging between 0.69 and 0.91 (significant at 90% confidence interval; Figs. 2c,d). The future–present climate difference looks very similar in CP4 and P25 (Fig. 2c). However, when comparing the CP4 (and P25) present-climate and future-climate simulations, correlations are high in November (0.8 and 0.71 respectively), but are much lower in other months (Fig. 2e, dashed lines). This is due to the fact that the boundary conditions differ between the present- and future-climate simulations; the extent of the impact of this depends on the consistency of the global climate response to common interannual SST anomalies. The experiment design (wherein future SST is formed of SST analyses plus average SST change; section 2) means that ENSO and IOD years are the same in the present and future scenarios. This explains the high correlation between present and future scenarios in the peak of the short rains (November), known to respond strongly to such events (Nicholson 2017), but in other months there is a different tropics-wide atmospheric response to the SSTs leading to different interannual variability in East African precipitation.

Correlations with observations (TAMSATv3) are weaker than the CP4/P25 correlations for most months (Fig. 2e), although correlation coefficients of 0.77 and 0.84 (CP4 and P25) for November indicate that the simulations are able to capture the observed interannual variability in the peak of the short rains. Correlation values for the long rains are lower (ranging from −0.2 to 0.52). This is related to the differing nature of the long and short rains; observational studies have found teleconnections between SSTs and the short rains, while correlations between the long rains and SSTs are much weaker (e.g., Walker et al. 2019). Vellinga and Milton (2018) found the seasonal amplitude of the Madden–Julian oscillation was associated with the interannual variability of the long rains (via changes in subsidence over East Africa). The high correlation between CP4 and P25 during the long rains indicates that March–May rainfall in the simulations is linked to their common boundary conditions, but this large-scale response to global SSTs differs in the real world due to random internal atmospheric variability, and hence the model and observation rainfall correlations are lower during the long rains. The high correlations during the short rains are likely to be the consequence of both model and observed rainfall being linked to specific SST patterns, such as the IOD, and consistent atmospheric responses to these SSTs and impact thereof on East Africa, which models are known to capture well.

b. Seasonal cycle: Present-day evaluation

Having determined that the interannual variability is similar in CP4 and P25 under present and future climates, in this section the representation of the 10-yr mean precipitation seasonality under present-climate conditions is explored.

Figures 3 and 4 show the mean annual cycle of precipitation over East Africa, and the mean onset and cessation dates over the region for both the present- and future-climate simulations. Onset and cessation dates were calculated using the method of anomalous accumulation (see section 2c; Liebmann et al. 2012; Dunning et al. 2016; Fig. S1 in the online supplemental material). Both simulations correctly capture the biannual seasonal cycle, with wet seasons in March–May (long rains) and October–December (short rains; Fig. 3a). However, there are differences between CP4/P25 and the observations (TRMM and TAMSATv3).

Both simulations overestimate the duration of the long rains, with the onset of the long rains too early and the end of the long rains too late (Figs. 3a and 4). This overestimate is more pronounced in P25; the stars in Fig. 4 demonstrate that the long-rains onset/cessation dates in P25 are statistically significantly different (paired difference test) from the long-rains onset/cessation dates in TAMSATv3. The rainfall peak in April is also higher in P25 than in TRMM, TAMSATv3, and CP4. However, in May the overestimate is slightly more pronounced in CP4 than in P25.

P25 also overestimates rainfall in September–October (Fig. 3a), and thus the onset of the short rains is too early in P25 (Fig. 4). The difference between the short-rains onset in P25 and TAMSATv3 is statistically significantly different (shown by the star). For the short rains, CP4 shows much better agreement with observations. This difference in the

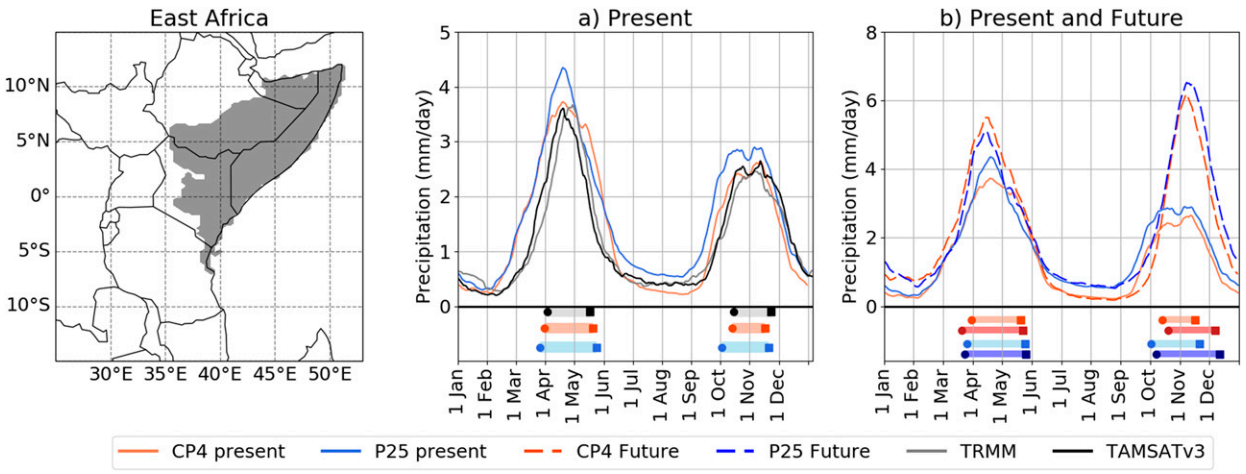

FIG. 3. Mean annual cycle of precipitation over East Africa (region shown on map to left): (a) Observed precipitation mean annual cycle (TAMSATv3 and TRMM) and mean annual cycle from present-climate simulations from CP4 and P25. (b) Mean annual cycle from present- and future-climate CP4 and P25 simulations (future-climate simulations are shown with dashed lines). Mean annual cycles were smoothed using a 31-day moving average. The shaded bars at the bottom show the mean period of the wet season, with circles and squares showing the mean onset and cessation dates, respectively; gray is for TAMSATv3, orange is for CP4, and blue is for P25. For (b) the darker bars are for the future-climate simulation.

representation of the onset of the short rains is the largest difference between CP4 and P25 for the present-climate simulations.

In both CP4 and P25 rainfall is higher in the long rains than the short rains, in agreement with observations, while Yang et al. (2015b) found large overestimates in the short rains in the AMIP models such that short rains rainfall was comparable with long rains rainfall. The better balance in rainfall amounts in CP4 and P25 may be related to the updated model versions [GA7/GL7 is the input for CMIP6, whereas Yang et al. (2015b) analyzed CMIP5 models] or the higher model resolution, or it may not be present in the MetUM [Hadley Centre models were not included in Yang et al.'s (2015b) analysis]. Dunning et al. (2017) found that the AMIP models overestimated the long rains (onset too early and cessation too late) and had too-late end of the short rains. The overestimate in the long rains was also found in both CP4 and P25, but CP4 had a much better representation of the short rains. This therefore suggests that CP4 has a better representation of the seasonal cycle, especially for the short rains, over East Africa than the AMIP models produced as part of the CMIP5 process. P25 offers some improvement, in that it correctly shows the long rains wetter than the short rains but has timing biases for both the long and short rains.

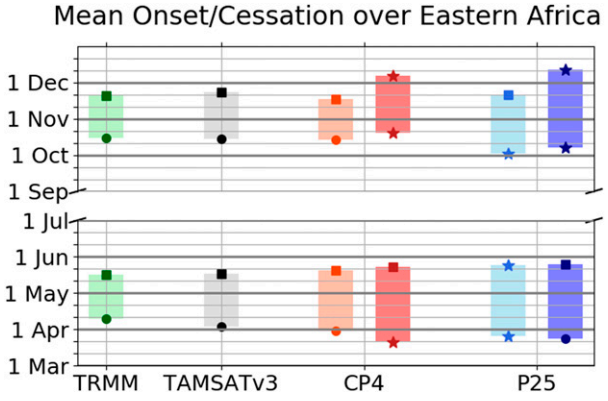

FIG. 4. Mean period of the wet season in observations (TAMSATv3 and TRMM), and the present- and future-climate CP4 and P25 simulations. The circles and squares respectively show the mean onset and cessation of the wet season averaged over 10 years and over the East African region shown in Fig. 2; the shaded bar shows the period of the wet season. For CP4 and P25 the darker bars show the future-climate simulations. Stars indicate statistically significant differences. On the present-climate (lighter) bars, the stars indicate if the onset/cessation is statistically significantly different from the onset/cessation from TAMSATv3. On the future-climate (darker) bars the stars indicate if the onset/cessation is statistically significantly different from the onset/cessation in the corresponding present-climate simulation. The paired difference test was used to establish statistical significance; see section 3e.

Overall, the main difference between CP4 and P25 in terms of present-climate seasonal cycles relates to the overestimate of rainfall in P25 in September–October, and the early onset of the short rains. This will be explored further in section 3d. Both simulations have smaller overestimates of the long rains with onset too early and cessation too late.

c. *Seasonal cycle: Future change*

Existing future projections of changing seasonality over East Africa have previously been produced using the CMIP5 models (e.g., Dunning et al. 2018), which do not correctly represent the current observed seasonal cycle over East Africa (Yang et al. 2015b). Therefore, having shown that CP4 and P25 capture the current seasonal cycle over East Africa better than the CMIP5 models, here we investigate the changing seasonality

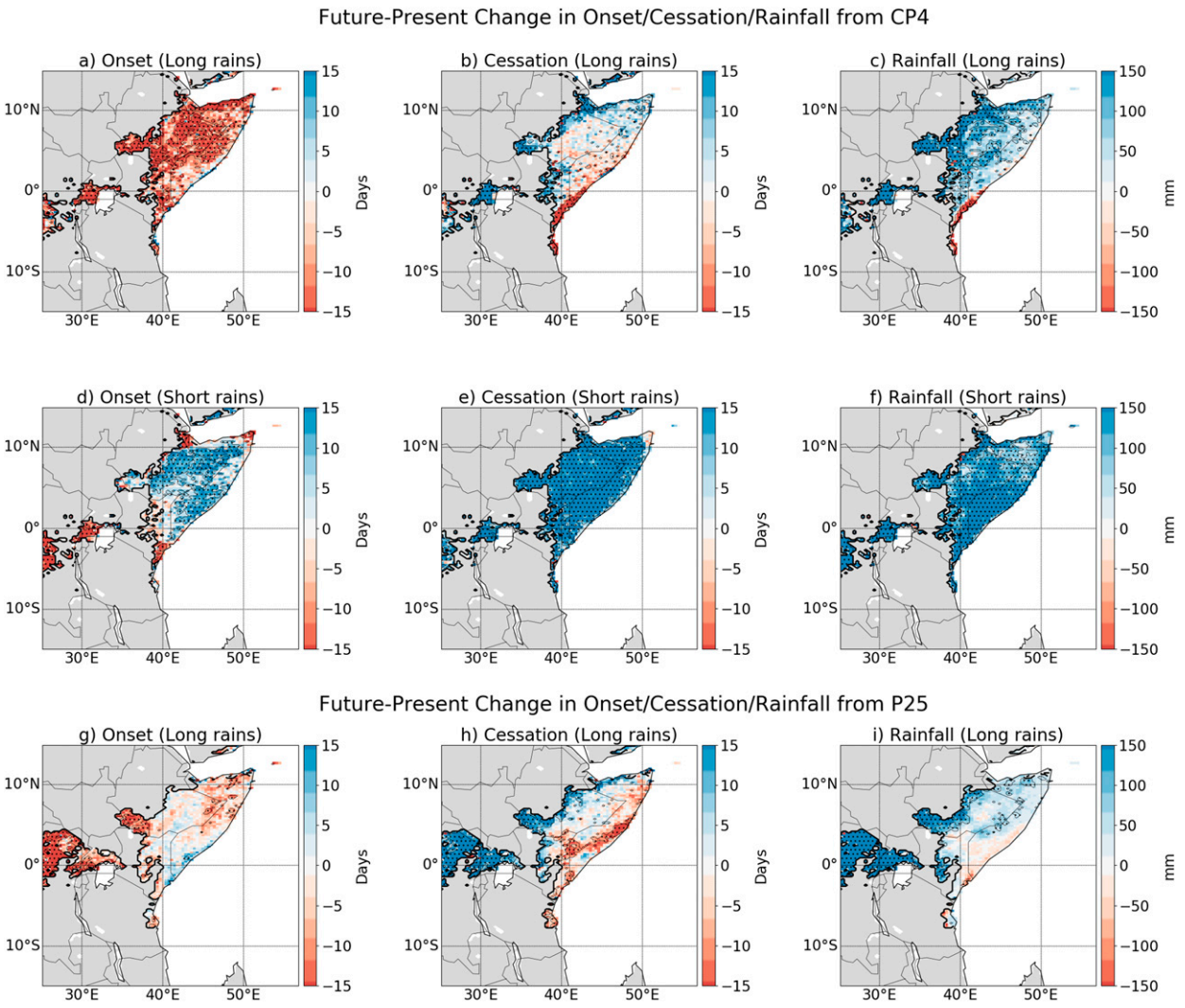

FIG. 5. Future-climate minus present-climate change in onset/cessation dates for the (top) and (bottom) long rains and (middle) short rains for (a)–(f) CP4 and (g)–(i) P25. Stippling indicates where the change is significant at the 10% significance level. Gray regions have one wet season per year.

signals in the CP4 and P25 models under future climate change, to establish if they agree with projections from CMIP5 simulations and whether explicit convection affects the climate change in the seasonal cycle. Furthermore, projections from the CP4 and P25 simulations are compared to establish the role of explicit convection on future projections of seasonality.

Figure 3b compares the seasonal cycle of precipitation under present and future climates. Both projections show a large increase in rainfall during the short rains, and a smaller increase in rainfall during the long rains. Given the role of remote drivers found above, the large increase in short rains rainfall may be linked to its strong association with SSTs, although the possibility of a consistent (year-to-year) role of processes within the East African region is also plausible [cf. Rowell and Chadwick's (2018) decomposition]. The peak of the short rains increases from 2.5–3 to ~6 mm day^{-1}. In the dry seasons, no increase is found in either simulation during the boreal summer, but small increases are seen in boreal winter; this is discussed further in section 3e. In terms of timing, there is an apparent shift in the timing of the peak of the short rains, occurring later in the future-climate simulation.

Figure 4 shows the timing of the onset and cessation of the long and short rains under both present and future climate; the darker bars are for the future-climate simulation. This confirms a change in the timing of the short rains; both P25 and CP4 project the onset and cessation of the short rains getting later under future climate change, with the change in cessation larger than the change in onset date, and thus a lengthening of the season. The stars indicate that the changes in onset/cessation of the short rains are statistically significant. For the long rains the changes in onset/cessation are much smaller; Fig. 4 shows that the only statistically significant change is the onset of the long rains getting earlier in the CP4 simulation.

Figure 5 and Fig. S2 in the online supplemental material depict the spatial pattern of the mean future-climate minus

present-climate changes in onset/cessation for the region that experiences a biannual regime; stippling indicates statistically significant changes. For the short rains, Figs. 5d–f and Fig. S2 show that the later onset and cessation and increase in seasonal rainfall are universal across the part of East Africa that experiences a biannual regime; the only differences are found over parts of Uganda where the short rains onset gets earlier; this will be discussed further in section 3e. These projections agree with the projections from the CMIP5 models (Dunning et al. 2018), which showed later onset and cessation of the short rains, and an increase in short rains rainfall (which was, for the ITCZ as a whole, linked to its slower retreat and a deepening of the Saharan heat low). For the short rains the projections in CP4 and P25 are very similar, suggesting that this response is not affected by the representation of convection.

For the long rains, Fig. 4 shows that CP4 projects the onset of the long rains getting earlier, whereas P25 shows little change in the timing of the long rains. Figure 5a shows the onset of the long rains in CP4 advancing by more than 10 days in some locations while P25 only contains small changes in the onset of the long rains under future climate change (Fig. 5g). The change in long rains onset in CP4 is statistically significant across much of the region (Fig. 5a), while there is no statistically significant change in P25. This earlier onset signal is a consequence of the rainfall increase in February and early March in CP4, shown in Fig. 3b. P25 does not show a rainfall increase in early March. For the cessation of the long rains, neither CP4 nor P25 shows a consistent signal; averaged across the region, changes are small, although there is a coherent picture of later long rains cessation in both models in Uganda. Both models show an increase in long rains rainfall (as in Fig. 3b), but this is much more widespread in CP4 than P25 (Fig. 5); the P25 increase is largest over the region north of Lake Victoria. Figs. 5c and 5i both show rainfall decreases along the coastline of the Horn of Africa, particularly in CP4, linking to the inland shift of sea breeze convergence described by Finney et al. (2020a).

Dunning et al. (2018) found that CMIP5 models projected the cessation of the long rains getting earlier, although fewer than 50% of the models used showed a statistically significant change. For the onset of the long rains and long rains rainfall Dunning et al. (2018) did not find strong model agreement; Rowell et al. (2015) also found that CMIP5 models do not agree on the sign of future rainfall change in March, April, and May. Therefore, both CP4 and P25 projections are within the range of CMIP5 projections. These results suggest that for the long rains the representation of convection does affect the projections of changing seasonality under future climate change, and this is potentially an additional source of uncertainty, not considered in projections based on CMIP/CORDEX alone.

Parts of western Kenya and Uganda are not included in Fig. 5; this is because harmonic analysis suggests that either in the present- or future-climate simulation these regions experience one wet season per year. The changing seasonality over these regions is explored in section 3e.

d. *Toward an understanding of current seasonality differences and future seasonality changes*

Results in section 3b show that both simulations correctly capture the biannual seasonal cycle over East Africa, with higher rainfall totals in the long rains than the short rains. In section 3c it was found that both simulations show the onset and cessation of the short rains getting later under future climate change, with an increase in short rains rainfall, as found in the CMIP5 projections (Dunning et al. 2018). In addition, two differences between the CP4 and P25 simulations have been identified in terms of seasonality of rainfall over East Africa:

1) P25 overestimates the rainfall in September–October, leading to an early onset of the short rains (under present climate), and
2) projections from CP4 show an earlier onset of the long rains under future climate change, whereas P25 shows little change in the onset of the long rains.

The precipitation annual cycle over East Africa has previously been associated with the convective instability (CI), and in particular, the annual cycle of near-surface moist static energy (MSE; Yang et al. 2015a). Furthermore, differences in the precipitation annual cycle in different model simulations could be explained by the bias in CI (Yang et al. 2015b). Therefore, in order to explore these differences between CP4 and P25, the annual cycle of CI is calculated for each simulation (see section 2d). The difference between the MSE of a rising parcel and the saturated MSE at a given height is proportional to the parcel's buoyancy (Cook and Seager 2013); therefore, smaller negative values of CI imply greater buoyancy and less stability and more convective rainfall.

Figure 6 shows the annual cycle in CI over East Africa, calculated as the difference (dotted line) between the surface MSE (h_s; solid line in Fig. 6a) and the saturated MSE at 700 hPa ($h^*_{700\text{hPa}}$; dash–dotted line in Fig. 6a), as defined in Yang et al. (2015a). As found in Yang et al. (2015a), the annual cycle of CI closely follows the annual cycle of rainfall, with peaks in April–May and October–November, and the annual cycle in CI is dominated by the surface MSE (which is then dominated by the surface specific humidity; Fig. S3 in the online supplemental material).

Previously, Yang et al. (2015b) found that the differences in the annual cycle of rainfall over East Africa between atmosphere-only and coupled models produced as part of CMIP5 could be explained by the bias in CI (dominated by the near-surface MSE). Figure 6b shows the present-climate CP4–P25 difference in h_s, $h^*_{700\text{hPa}}$, CI, and precipitation; blue shading indicates CI is higher in P25, and orange indicates CI is higher in CP4. CI is higher in P25 than in CP4 in April and June–October and rainfall is higher in P25 than in CP4 for April and mid-June–December (Figs. 3 and 6b). Therefore, Fig. 6b shows that periods with higher CI in P25 mostly agree with periods of higher rainfall in P25. This higher CI in P25 is mostly due to higher surface MSE; surface MSE is higher in P25 than in CP4 for March–December. This must be because although the SSTs in the models are identical, the models differ in their circulation and surface energy balance, affecting the low-level MSE (Finney et al. 2019). In May, while h_s is higher in P25 than in CP4, $h^*_{700\text{hPa}}$ is much lower in CP4, leading to higher CI in CP4, consistent with more precipitation in May in CP4 than in P25. The largest differences in h_s are in April and September–October; P25 has more than 2 mm day^{-1} more rainfall than

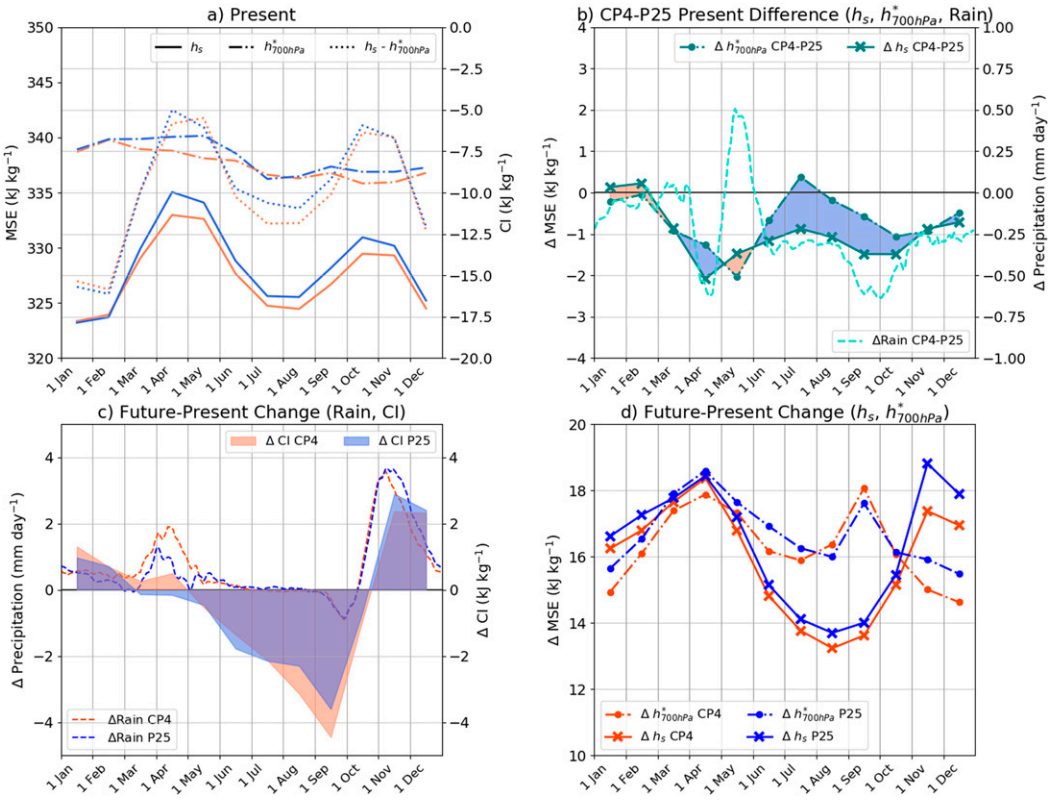

FIG. 6. (a) Annual cycle of surface MSE (h_s; solid lines and left axis), saturated MSE at 700 hPa ($h^*_{700\text{hPa}}$; dash–dotted lines and left axis), and convective instability ($h_s - h^*_{700\text{hPa}}$; dotted line and right axis) in CP4 and P25 over East Africa (region shown in gray in Figs. 2 and 3) under present-climate. (b) CP4 − P25 present-climate difference in h_s, $h^*_{700\text{hPa}}$, and precipitation. The shading shows the difference in CI; blue shading indicates that CI is higher in P25 and orange/red indicates that CI is higher in CP4. (c) Future-climate minus present-climate change in convective instability in P25 and CP4 (shading) and precipitation (dashed line). (d) Future-climate minus present-climate change in surface MSE (solid line) and saturated MSE at 700 hPa (dash–dotted line) for CP4 and P25.

CP4 in April and September–October. Therefore, the rainfall overestimate and early onset of the short rains in P25 appear to be related to higher CI and higher surface MSE, again likely related to the differences in circulation and surface energy balance between the models.

The difference in monthly rainfall, surface MSE, temperature, and specific humidity for September and October are shown in Fig. 7. The higher rainfall totals in P25 are located over the central Horn of Africa; in other areas CP4 has higher rainfall (e.g., over the northern Ethiopian Highlands; Figs. 7a,b). This region of higher rainfall in P25 is collocated with the region of higher surface MSE, particularly in October (Figs. 7c,d). Breaking surface MSE into its components of temperature and specific humidity, Figs. 7e and 7f show opposite and small temperature differences across the Horn of Africa in September and October. On the other hand, Figs. 7g and 7h show higher specific humidity in P25 over the central Horn of Africa, over the same region that has higher MSE and rainfall. Thus, this suggests that the higher rainfall in P25 may be linked to higher surface MSE, and higher specific humidity. Furthermore, Fig. S3 in the online supplemental material shows differences in $L_v q$ between CP4 and P25 of similar magnitude to the differences in surface MSE, while the differences in $c_p T$ are of much smaller magnitude. This supports the proposal that the difference in surface MSE is linked to differences in specific humidity. However, this higher specific humidity (and MSE) could be a consequence of the higher rainfall. Further analysis is required to investigate causality. Initial analysis of the differences in vertically integrated moisture flux between CP4 and P25 showed only small differences (result not shown).

Figure 6 also shows the change in CI and MSE for the future climate simulation (Figs. 6c,d). Under increasing greenhouse gas concentrations and rising temperatures, CI decreases in May–October and increases in November–February, consistent with the signal of the onset of the short rains getting later and more rainfall during the short rains and January (Figs. 3 and 4). Figure 6d shows the future-climate minus present-climate change in h_s and $h^*_{700\text{hPa}}$. From June to October the increase in $h^*_{700\text{hPa}}$ is greater than the increase in h_s; therefore, the CI decreases and there is no increase in boreal summer rainfall, and rainfall decreases in September–early October (Fig. 6c). There is a particularly pronounced increase in $h^*_{700\text{hPa}}$ in September. In November–January the increase in h_s is

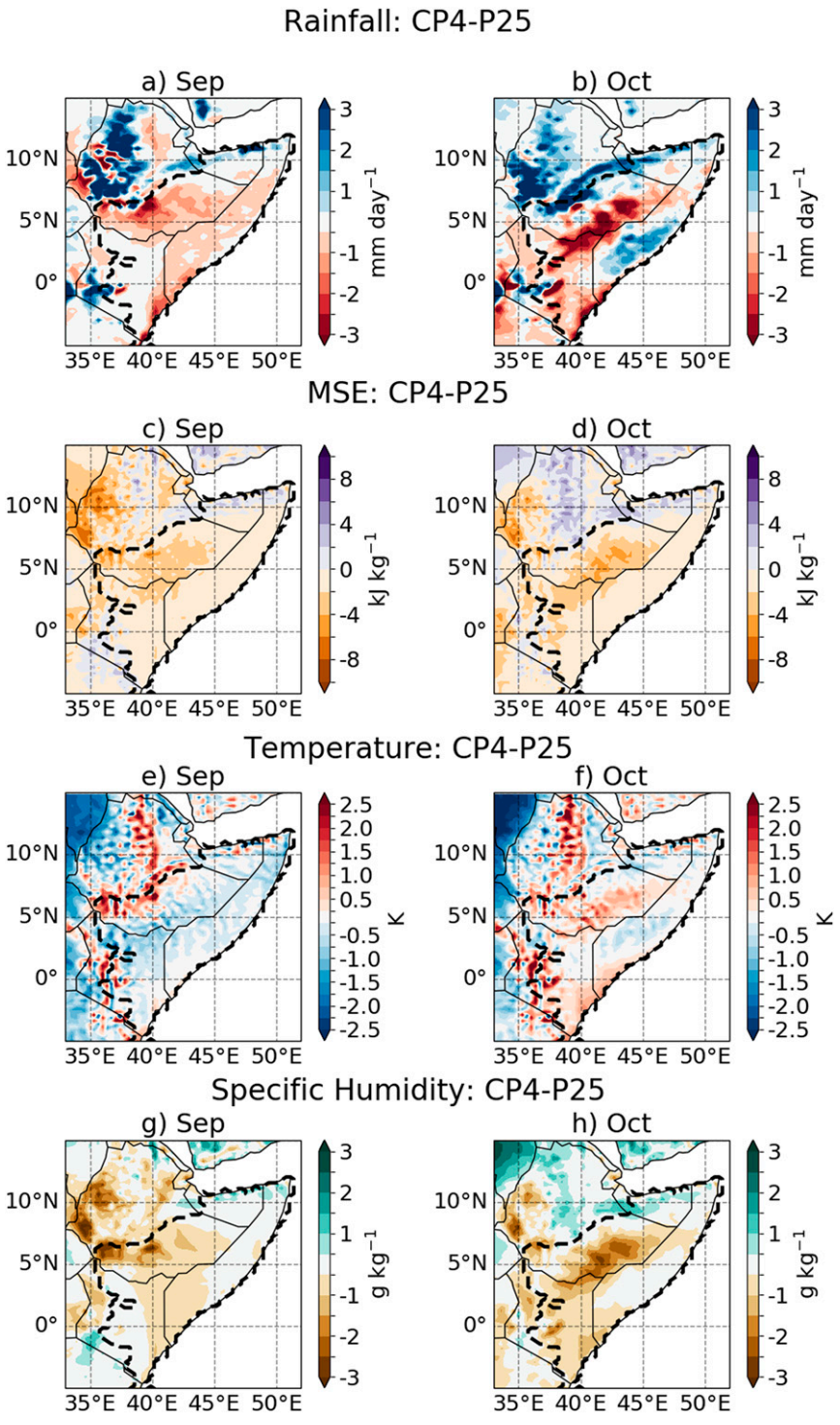

FIG. 7. Monthly differences between CP4 and P25 for (left) September and (right) October in (a),(b) rainfall; (c),(d) surface MSE; (e),(f) temperature; and (g),(h) specific humidity. The dashed black contour marks the East Africa region used in this study.

greater than the increase in $h^*_{700\text{hPa}}$, and there are corresponding rainfall increases.

In section 3c it was found that future-climate projections from CP4 show the onset of the long rains getting earlier, while projections from P25 do not (Figs. 4 and 5). Figure 6c shows a slight increase in CI in CP4 in January–April, whereas in P25 there is an increase in January–February only. Correspondingly, Fig. 6d shows the increase in h_s is marginally higher than the increase in $h^*_{700\text{hPa}}$ for CP4 during March–April, while the increases in h_s and $h^*_{700\text{hPa}}$ are very similar in P25 during March–April. This larger increase in h_s than in $h^*_{700\text{hPa}}$ is consistent with larger rainfall increases in CP4 than in P25, and the earlier onset. CP4 also contains a larger increase in surface specific humidity in March and April than in P25 (not shown). However, the increase in CI in CP4 in March–April is small; the difference in onset projections may be related to the convective response to the environment change and ability of the model to trigger convection; the convection-permitting model UM has triggering more coupled to mesoscale convergence (Birch et al. 2014b), which may lead to an increase in rainfall in March that leads to an earlier onset. Further work is required to explore this difference further, as changes in the CI may not fully explain precipitation changes.

e. *Local changes in seasonality*

In section 3c the focus was on changes in the timing and totals of wet season rainfall across East Africa under future climate change. This does not however address larger but more local changes in the shape of the seasonal cycle, which may have large socioeconomic consequences. In addition, the analysis in section 3c excluded regions, such as parts of western Kenya and Uganda, that do not experience a well-defined biannual seasonal cycle with two equinoctial rainy seasons. Both P25 and CP4 have much higher horizontal resolution than the majority of climate model simulations, which enables us to explore small regions with specific seasonal regimes, and possible changes in these regimes under future climate change. Therefore, in this section we explore changes in the shape of the seasonal cycle. The results are split into two sections: changes in the January–February dry season and changes in boreal summer/autumn rainfall.

1) RAINFALL INCREASES IN THE JANUARY–FEBRUARY DRY SEASON

Figure 6 shows increases in the CI and rainfall in January–February (JF). Rowell et al. (2015) and IPCC projections (Collins et al. 2013) both found increases in JF rainfall across the Horn of Africa. Recently, above average rainfall in January 2020 over Kenya, following an above average short rains, had significant impacts (Wainwright et al. 2020). Therefore here we explore the projected changes in the JF dry season.

Figures 8a and 8b show the ratio of the mean daily rainfall in JF to the mean daily rainfall in November (the peak month of the short rains) in CP4 under present climate (Fig. 8a) and future climate (Fig. 8b). Figure S4 in the online supplemental material is the corresponding plot for P25 and shows similar results. The pink colors across much of East Africa (excluding Tanzania) show that currently the mean daily rainfall is lower in JF than in November (Fig. 8a). Figure 8b shows that we expect JF to remain drier than November under future climate change, and Fig. 8c confirms that the difference in ratios is small. However, Fig. 8d shows that increases in JF rainfall mean that across much of Kenya and central Ethiopia the mean daily rainfall in JF in the future will be greater than, or comparable to, the mean daily rainfall in present-climate peak of the short rains (November). The mean annual cycles in Figs. 8e and 8f demonstrate this; over the region in Fig. 8e (Fig. 8f) the mean daily rainfall in JF under future climate will be around 1 mm day^{-1} (4 mm day^{-1}), whereas under present climate the mean daily rainfall in November is also around 1 mm day^{-1} (4 mm day^{-1}). CP4 and P25 both show increases in JF rainfall across East Africa (Fig. S5 in the online supplemental material). Over parts of southern Kenya (Fig. 8f) it could be interpreted that the seasonal cycle is changing from a biannual regime with two wet seasons per year to an annual regime with one long austral summer wet season with a midseason quasi-dry period in JF, which is still much wetter than the annual dry season of June to September. Further analysis of mechanisms and changes in CP4, P25, and CMIP5/6 models should be completed to further explore changes in the JF dry season.

2) INCREASES IN BOREAL SUMMER/AUTUMN RAINFALL

While the Horn of Africa experiences two equinoctial wet seasons per year (long rains and short rains) the seasonal cycle over western Kenya and Uganda is different. These regions do experience rainfall during March–May and October–December, but they also experience rainfall during the boreal summer (Fig. 9). Finney et al. (2020b) find that a westerly moisture flux over East Africa enhances rainfall during the boreal summer. Currently, western Kenya experiences a pronounced long rains wet season in March–May (MAM), and then wet conditions through to November, followed by a dry season in December–January (Figs. 9a,b, solid lines). Over Uganda the wet season starts in March and persists until November, with a midseason drier period from June to August (Fig. 9c, solid lines). Under future climate change both regions and simulations show rainfall increases throughout the year, with especially large increases during October–November, particularly in CP4, which may be related to the higher-resolution topography in CP4 (dashed lines in Fig. 9). The increases in June–September rainfall are also much higher in CP4 than in P25. Figure S6 in the online supplemental material shows the CP4–P25 difference in future projections of mean daily rainfall in each month; in most months CP4 shows larger rainfall increases over western Kenya and Uganda than P25. Over western Kenya, rainfall totals during the short rains are currently lower than during the boreal summer season; however, Fig. 9a suggests that under future climate change the short rains could be much wetter than the boreal summer wet season.

To examine the spatial extent of these changes, the ratio of the mean rainfall in June–September (JJAS) to the mean rainfall in October–December (OND) and MAM, and the ratio of the mean rainfall in MAM to the mean rainfall in OND, were computed for CP4 and P25 in present and future climates, and the ratios were compared (Fig. 10 and Fig. S7 in the online supplemental material). Across most of East Africa

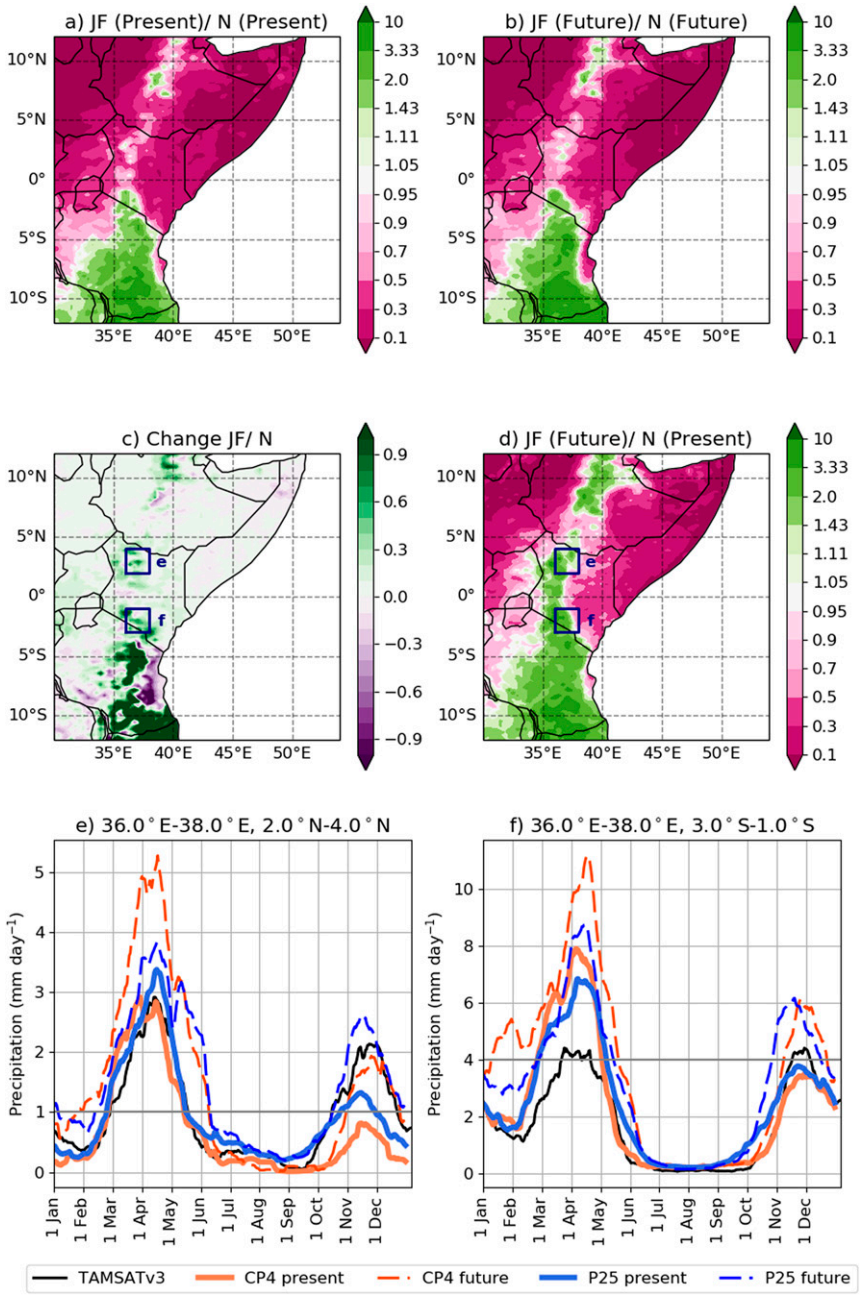

FIG. 8. Changes in the January–February (JF) dry season: the ratio of mean daily rainfall in JF to mean daily rainfall in November in CP4 under (a) present climate and (b) future climate, (c) the change in ratio from present- to future-climate for CP4 [(b) minus (a)], (d) the ratio of mean rainfall in JF in the future-climate simulation to mean rainfall in November in the present-climate simulation for CP4, and (e),(f) the mean annual cycle in precipitation over two regions in western and southern Kenya [the regions outlined in (c) and (d)] for the present- and future-climate simulations for CP4 and P25, and observations from TAMSATv3.

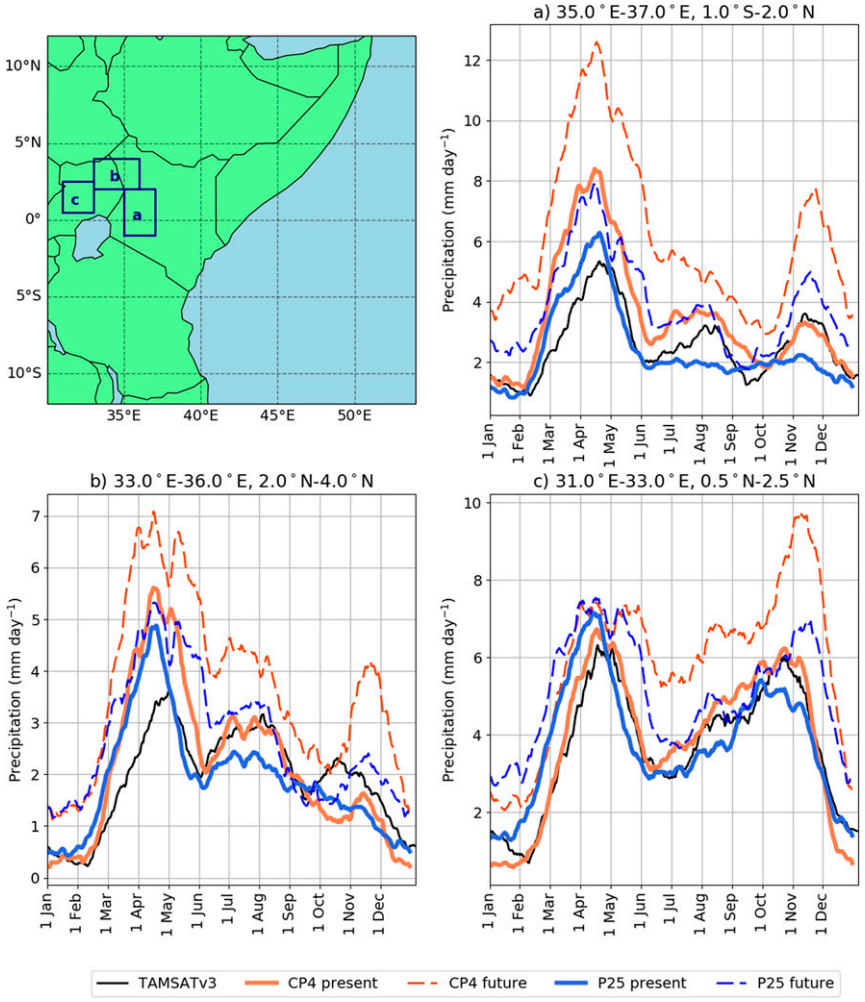

FIG. 9. Mean annual cycle in precipitation over three regions in Uganda/western Kenya (regions shown in the map at the top left) for the present- and future-climate simulations for CP4 and P25, and observations from TAMSATv3.

the mean rainfall is lower in JJAS than in MAM (Fig. 10a), and this is expected to persist under future climate change (Fig. 10b); Fig. 10c shows little change in the JJAS/MAM ratio. The results are similar in P25 (Figs. S7a–c). Currently most of East Africa experiences higher mean rainfall during OND than during JJAS; however, the green colors in Fig. 10d indicate that western Kenya and Uganda experience higher mean rainfall in JJAS than in OND. In Fig. 10e the green region has contracted and Fig. 10f shows a decrease in the JJAS:OND ratio over western Kenya and Uganda, and to the north over Ethiopia. This indicates that under future climate change over these regions the increase in OND rainfall is greater than the increase in JJAS rainfall, and over some regions the balance of rainfall in these seasons will change (as seen in Figs. 9a,b). In P25 (Fig. S7) a decrease in the ratio is still present but smaller than in CP4, consistent with the smaller increases in P25 shown in Fig. 9.

Figure 10 also shows the change in the MAM:OND ratio; currently rainfall totals are higher during the long rains than during the short rains, however, the decreasing ratio across East Africa shows that increases during the short rains will be greater than during the long rains, with the short rains becoming wetter than the long rains in some regions (as seen in Fig. 3, also found in P25: Figs. S7g–i). This change in the dominant season from the long rains to the short rains along the Somali coast was also found by Kendon et al. (2019).

The changing seasonality identified here needs to be considered in adaptation planning and flood management, as wetter "dry seasons" and heavy rainfall at the end of a prolonged wet season may lead to more runoff and flooding events.

4. Conclusions

In this study we investigated the role of explicit versus parameterized convection on the representation of precipitation seasonality over East Africa under present climatic conditions and on projections of changing seasonality under future climate change. This was achieved using new high-resolution

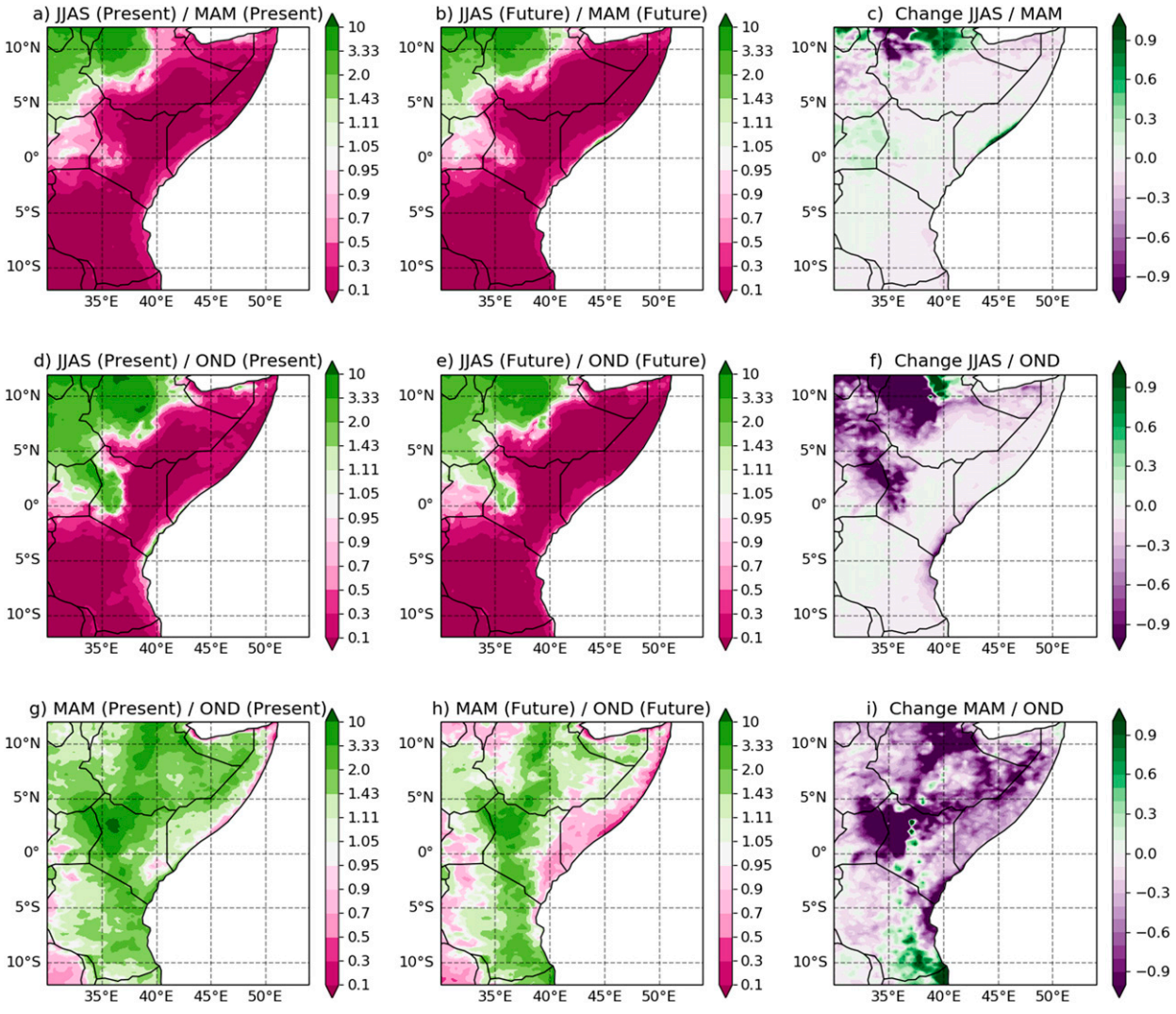

FIG. 10. Ratio of the mean daily rainfall in different seasons for CP4 under (left) present and (center) future climate, and (right) the future minus present change, showing (a)–(c) the ratio of mean rainfall in June–September (JJAS) to mean rainfall in March–May (MAM), (d)–(f) the ratio of mean rainfall in JJAS to mean rainfall in October–December (OND), and (g)–(i) the ratio of mean rainfall in MAM to mean rainfall in OND.

regional model simulations, including the first pan-African climate change simulations that explicitly model convection, produced as part of the FCFA IMPALA project.

First, it is shown that the interannual variability in the two (CP4 and P25) present-climate and two future-climate simulations is very similar, with high monthly rainfall correlations in the wet season months (March, April, May, October, November, and December) and in January–February. This indicates that the modeled interannual variability in these simulations is primarily controlled by the boundary conditions from the global driving model (including SSTs), and only marginally influenced by the representation of convection and factors within the regional domain, and that modeling observed regional interannual variability is not significantly improved by explicit convection over an African domain.

Second, analysis of the present-climate simulations shows that CP4 and P25 both capture the biannual seasonal cycle over East Africa better than is typically the case for global climate models, with higher rainfall totals in the long rains than the short rains. However, both overestimate the long rains, and P25 overestimates rainfall in September and October, giving a too early start to the short rains. In contrast, the onset of the short rains in CP4 shows good agreement with observations. This difference in the representation of the onset of the short rains is the main difference between CP4 and P25 for the present-climate simulations. The overestimate in P25 is associated with higher convective instability and surface moist static energy in September–October. Spatially, the regions with higher rainfall in P25 in September and October also exhibit higher surface MSE and higher specific humidity, although further work is required to establish causality.

Under future climate change CP4 and P25 show the onset and cessation of the short rains getting later under future climate change, with a large increase in short rains rainfall, in agreement with the multimodel mean projections from the CMIP5 models (Dunning et al. 2018). Convective instability decreases in September–October and increases in November–December, consistent with the short rains getting later and increasing short rains rainfall.

For the long rains, CP4 shows the onset of the long rains getting earlier, while P25 shows little change in the onset of the long rains over East Africa; also, CP4 shows larger rainfall increases in February–April. CP4 shows a slight increase in CI in January–April while P25 shows an increase in January–February only; however, the CI increase in CP4 is small and further work is required to explore this. Both models show a later long rains cessation to the north of Lake Victoria, but this change is not seen across the rest of the East African region. This study has shown that while the representation of convection does not affect the more robust short rains projections, it does affect the more variable long rains projections in these simulations. This is an important result as understanding recent trends and future projections of the long rains over East Africa remains a significant challenge (Rowell et al. 2015; Wainwright et al. 2019). These results are consistent with the strong role of SST forcing during the short rains, and more subtle convective processes such as the Madden–Julian oscillation during the long rains (Vellinga and Milton 2018; Finney et al. 2020b).

Unlike the rest of East Africa, western Kenya and Uganda do not exhibit a biannual seasonal regime with two equinoctial wet seasons. Under present climate, rainfall starts in March and continues throughout the boreal summer to November, followed by a dry season in December–January. Currently mean rainfall is higher during the boreal summer (JJAS) than during the short rains (OND). Under future climate change proportionally larger increases in short rains rainfall lead to changes in the shape of the seasonal cycle, with the currently drier short rains becoming wetter than the boreal summer wet season. These changes in the shape of the seasonal cycle are more pronounced in CP4 than in P25. In other regions, increases in January–February rainfall are found, such that mean rainfall in January–February under the future climate is higher than mean rainfall during the peak of the short rains under the present climate. These changes in the shape of the seasonal cycle have the potential for large socioeconomic impacts. The convection-permitting model (CP4) shows much larger changes, which would have significant societal impacts. The increases in P25 are much smaller over these parts of western Kenya and Uganda. However, it should be noted that these are the results from a single model; other models should be examined to establish the robustness of these conclusions. Further work also is required to ascertain the drivers behind the difference in the projections over this region.

The CP4 and P25 simulations are the first pan-African climate change simulations that explicitly model convection, and thus comprise an invaluable dataset for exploring the impacts of convective parameterization on model representation of African weather. High computational cost restricted the length of the simulations to 10 years. While this is sufficient for initial analysis of the seasonality, a longer dataset (or additional ensemble members) would enable more robust statistical testing of differences between the models. The two models showed differences in the projections of the long rains, but also contained differences in the long rains interannual variability under present- and future-climates, which may impact the projections. Longer simulations would reduce the impact of the differing interannual variability and may give a clearer climate change signal for the long rains, an important outcome, given the high socioeconomic importance of the long rains, and current uncertainty in future projections (Rowell et al. 2015). Longer simulations would also enable investigation of changing year-to-year variability in seasonality.

We also identified changes in the shape of the seasonal cycle over western Kenya and Uganda, and differences in the projections from the two models. Further work should explore this result in more detail and investigate the drivers and robustness of such changes using an ensemble of models. Changes in the shape of the seasonal cycle and increasing year-to-year variability in seasonality have high potential for detrimental socioeconomic consequences, as agricultural practices are strongly tied to the seasonal cycle of rainfall. Further exploration of such changes will provide important information for successful adaptation to future changes in climate over East Africa. It is also notable that many climate studies present changes in rainfall in fixed months or seasons, and do not relate the changes in different seasons to explain the changing seasonality. For many users changing seasonality will be critical, and presentations of possible future climate changes for such users should be designed to show this. It is important to note that all the projections presented here are based on output from a single coupled model (HadGEM2-ES) that has been shown to have high transient climate response compared to other CMIP5 models (Senior et al. 2016) (although less high relative to the updated CMIP6 ensemble; Tokarska et al. 2020), and, along with other CMIP5 models, fails to correctly capture the current seasonal cycle over East Africa (Dike et al. 2015); further work with an ensemble of models from a range of modeling centers is required to establish the robustness of these potentially important results.

Acknowledgments. We thank three anonymous reviewers for their helpful and constructive comments. Authors Caroline Wainwright, Declan Finney, John Marsham, David Rowell, and Emily Black were supported by the Natural Environment Research Council/Department for International Development (NERC/DFID, NE/M020371/1, NE/M02038X/1, and NE/M019985/1) via the Future Climate for Africa (FCFA) funded project, Integrating Hydro-Climate Science into Policy Decisions for Climate-Resilient Infrastructure and Livelihoods in East Africa (HyCRISTAL). John Marsham and Emily Black were also supported by the National Centre for Atmospheric Science via the NERC/GCRF programme Atmospheric Hazard in Developing Countries: Risk Assessment and Early Warning (ACREW). Emily Black also gratefully acknowledges support from the NERC/DFID BRAVE project (NE/M008983/1) and the Global Challenges Research Fund project, SatWIN-ALERT (NE/R014116/1).

Data availability statement. The CP4A dataset generated under the FCFA IMPALA project is publicly available, with currently a limited set of monthly mean variables downloadable from the Centre for Environmental Data Analysis (CEDA) archive (http://archive.ceda.ac.uk/; search for CP4A).

The TAMSAT data are publicly available from https://www.tamsat.org.uk/. The TRMM data are publicly available from https://gpm.nasa.gov/trmm.

REFERENCES

Ayugi, B., G. Tan, G. T. Gnitou, M. Ojara, and V. Ongoma, 2020: Historical evaluations and simulations of precipitation over East Africa from Rossby Centre regional climate model. *Atmos. Res.*, **232**, 104705, https://doi.org/10.1016/j.atmosres.2019.104705.

Berthou, S., E. Kendon, D. Rowell, M. Roberts, S. Tucker, and R. Stratton, 2019a: Larger future intensification of rainfall in the West African Sahel in a convection-permitting model. *Geophys. Res. Lett.*, **46**, 13 299–13 307, https://doi.org/10.1029/2019GL083544.

——, D. P. Rowell, E. J. Kendon, M. J. Roberts, R. A. Stratton, J. A. Crook, and C. Wilcox, 2019b: Improved climatological precipitation characteristics over West Africa at convection-permitting scales. *Climate Dyn.*, **53**, 1991–2001, https://doi.org/10.1007/s00382-019-04759-4.

Birch, C. E., D. Parker, J. Marsham, D. Copsey, and L. Garcia-Carreras, 2014a: A seamless assessment of the role of convection in the water cycle of the West African monsoon. *J. Geophys. Res. Atmos.*, **119**, 2890–2912, https://doi.org/10.1002/2013JD020887.

——, J. H. Marsham, D. J. Parker, and C. M. Taylor, 2014b: The scale dependence and structure of convergence fields preceding the initiation of deep convection. *Geophys. Res. Lett.*, **41**, 4769–4776, https://doi.org/10.1002/2014GL060493.

Clark, P., N. Roberts, H. Lean, S. P. Ballard, and C. Charlton-Perez, 2016: Convection-permitting models: A step-change in rainfall forecasting. *Meteor. Appl.*, **23**, 165–181, https://doi.org/10.1002/met.1538.

Collins, M., and Coauthors, 2013: Long-term climate change: Projections, commitments and irreversibility. *Climate Change 2013: The Physical Science Basis*, Cambridge University Press, 1029–1136.

Cook, B., and R. Seager, 2013: The response of the North American monsoon to increased greenhouse gas forcing. *J. Geophys. Res. Atmos.*, **118**, 1690–1699, https://doi.org/10.1002/jgrd.50111.

Crook, J., C. Klein, S. Folwell, C. M. Taylor, D. J. Parker, R. Stratton, and T. Stein, 2019: Assessment of the representation of West African storm lifecycles in convection-permitting simulations. *Earth Space Sci.*, **6**, 818–835, https://doi.org/10.1029/2018EA000491.

De Kauwe, M. G., C. M. Taylor, P. P. Harris, G. P. Weedon, and R. J. Ellis, 2013: Quantifying land surface temperature variability for two Sahelian mesoscale regions during the wet season. *J. Hydrometeor.*, **14**, 1605–1619, https://doi.org/10.1175/JHM-D-12-0141.1.

Dike, V. N., M. H. Shimizu, M. Diallo, Z. Lin, O. K. Nwofor, and T. C. Chineke, 2015: Modelling present and future African climate using CMIP5 scenarios in HadGEM2-ES. *Int. J. Climatol.*, **35**, 1784–1799, https://doi.org/10.1002/joc.4084.

Dinku, T., P. Ceccato, E. Grover-Kopec, M. Lemma, S. Connor, and C. Ropelewski, 2007: Validation of satellite rainfall products over East Africa's complex topography. *Int. J. Remote Sens.*, **28**, 1503–1526, https://doi.org/10.1080/01431160600954688.

Dosio, A., R. G. Jones, C. Jack, C. Lennard, G. Nikulin, and B. Hewitson, 2019: What can we know about future precipitation in Africa? Robustness, significance and added value of projections from a large ensemble of regional climate models. *Climate Dyn.*, **53**, 5833–5858, https://doi.org/10.1007/s00382-019-04900-3.

Dunning, C. M., E. C. Black, and R. P. Allan, 2016: The onset and cessation of seasonal rainfall over Africa. *J. Geophys. Res. Atmos.*, **121**, 11 405–11 424, https://doi.org/10.1002/2016JD025428.

——, R. P. Allan, and E. Black, 2017: Identification of deficiencies in seasonal rainfall simulated by CMIP5 climate models. *Environ. Res. Lett.*, **12**, 114001, https://doi.org/10.1088/1748-9326/aa869e.

——, E. Black, and R. P. Allan, 2018: Later wet seasons with more intense rainfall over Africa under future climate change. *J. Climate*, **31**, 9719–9738, https://doi.org/10.1175/JCLI-D-18-0102.1.

Finney, D. L., and Coauthors, 2019: Implications of improved representation of convection for the East Africa water budget using a convection-permitting model. *J. Climate*, **32**, 2109–2129, https://doi.org/10.1175/JCLI-D-18-0387.1.

——, J. H. Marsham, D. P. Rowell, E. J. Kendon, S. O. Tucker, R. A. Stratton, and L. S. Jackson, 2020a: Effects of explicit convection on future projections of mesoscale circulations, rainfall, and rainfall extremes over eastern Africa. *J. Climate*, **33**, 2701–2718, https://doi.org/10.1175/JCLI-D-19-0328.1.

——, ——, D. P. Walker, C. E. Birch, B. J. Woodhams, L. S. Jackson, and S. Hardy, 2020b: The effect of westerlies on East African rainfall and the associated role of tropical cyclones and the Madden–Julian oscillation. *Quart. J. Roy. Meteor. Soc.*, **146**, 647–664, https://doi.org/10.1002/qj.3698.

Fitzpatrick, R. G., and Coauthors, 2020: What drives the intensification of mesoscale convective systems over the West African Sahel under climate change? *J. Climate*, **33**, 3151–3172, https://doi.org/10.1175/JCLI-D-19-0380.1.

Gebrechorkos, S. H., S. Hülsmann, and C. Bernhofer, 2019: Regional climate projections for impact assessment studies in East Africa. *Environ. Res. Lett.*, **14**, 044031, https://doi.org/10.1088/1748-9326/ab055a.

Giorgi, F., C. Jones, and G. R. Asrar, 2009: Addressing climate information needs at the regional level: The CORDEX framework. *WMO Bull.*, **58**, 175, https://public.wmo.int/en/bulletin/addressing-climate-information-needs-regional-level-cordex-framework.

Huffman, G. J., and Coauthors, 2007: The TRMM Multisatellite Precipitation Analysis (TMPA): Quasi-global, multiyear, combined-sensor precipitation estimates at fine scales. *J. Hydrometeor.*, **8**, 38–55, https://doi.org/10.1175/JHM560.1.

Kendon, E. J., R. A. Stratton, S. Tucker, J. H. Marsham, S. Berthou, D. P. Rowell, and C. A. Senior, 2019: Enhanced future changes in wet and dry extremes over Africa at convection-permitting scale. *Nat. Commun.*, **10**, 1794, https://doi.org/10.1038/s41467-019-09776-9.

Kilavi, M., and Coauthors, 2018: Extreme rainfall and flooding over central Kenya including Nairobi city during the long-rains season 2018: Causes, predictability, and potential for early warning and actions. *Atmosphere*, **9**, 472, https://doi.org/10.3390/atmos9120472.

Liebmann, B., I. Bladé, G. N. Kiladis, L. M. Carvalho, G. B. Senay, D. Allured, S. Leroux, and C. Funk, 2012: Seasonality of African precipitation from 1996 to 2009. *J. Climate*, **25**, 4304–4322, https://doi.org/10.1175/JCLI-D-11-00157.1.

Maidment, R. I., and Coauthors, 2017: A new, long-term daily satellite-based rainfall dataset for operational monitoring in Africa. *Sci. Data*, **4**, 170063, https://doi.org/10.1038/sdata.2017.63.

Marsham, J. H., N. S. Dixon, L. Garcia-Carreras, G. M. Lister, D. J. Parker, P. Knippertz, and C. E. Birch, 2013: The role of moist

convection in the West African monsoon system: Insights from continental-scale convection-permitting simulations. *Geophys. Res. Lett.*, **40**, 1843–1849, https://doi.org/10.1002/grl.50347.

Mumo, L., and J. Yu, 2020: Gauging the performance of CMIP5 historical simulation in reproducing observed gauge rainfall over Kenya. *Atmos. Res.*, **236**, 104808, https://doi.org/10.1016/j.atmosres.2019.104808.

Nicholson, S. E., 2017: Climate and climatic variability of rainfall over eastern Africa. *Rev. Geophys.*, **55**, 590–635, https://doi.org/10.1002/2016RG000544.

Ongoma, V., H. Chen, and C. Gao, 2018: Projected changes in mean rainfall and temperature over East Africa based on CMIP5 models. *Int. J. Climatol.*, **38**, 1375–1392, https://doi.org/10.1002/joc.5252.

——, ——, and ——, 2019: Evaluation of CMIP5 twentieth century rainfall simulation over the equatorial East Africa. *Theor. Appl. Climatol.*, **135**, 893–910, https://doi.org/10.1007/s00704-018-2392-x.

Pearson, K., R. Hogan, R. Allan, G. Lister, and C. Holloway, 2010: Evaluation of the model representation of the evolution of convective systems using satellite observations of outgoing longwave radiation. *J. Geophys. Res.*, **115**, D20206, https://doi.org/10.1029/2010JD014265.

——, G. Lister, C. Birch, R. Allan, R. Hogan, and S. Woolnough, 2014: Modelling the diurnal cycle of tropical convection across the 'grey zone'. *Quart. J. Roy. Meteor. Soc.*, **140**, 491–499, https://doi.org/10.1002/qj.2145.

Prein, A. F., and Coauthors, 2015: A review on regional convection-permitting climate modeling: Demonstrations, prospects, and challenges. *Rev. Geophys.*, **53**, 323–361, https://doi.org/10.1002/2014RG000475.

Reynolds, R. W., T. M. Smith, C. Liu, D. B. Chelton, K. S. Casey, and M. G. Schlax, 2007: Daily high-resolution-blended analyses for sea surface temperature. *J. Climate*, **20**, 5473–5496, https://doi.org/10.1175/2007JCLI1824.1.

Rowell, D. P., and R. Chadwick, 2018: Causes of the uncertainty in projections of tropical terrestrial rainfall change: East Africa. *J. Climate*, **31**, 5977–5995, https://doi.org/10.1175/JCLI-D-17-0830.1.

——, B. B. Booth, S. E. Nicholson, and P. Good, 2015: Reconciling past and future rainfall trends over East Africa. *J. Climate*, **28**, 9768–9788, https://doi.org/10.1175/JCLI-D-15-0140.1.

Senior, C. A., and Coauthors, 2016: Idealized climate change simulations with a high-resolution physical model: HadGEM3-GC2. *J. Adv. Model. Earth Syst.*, **8**, 813–830, https://doi.org/10.1002/2015MS000614.

Sherwood, S. C., S. Bony, and J.-L. Dufresne, 2014: Spread in model climate sensitivity traced to atmospheric convective mixing. *Nature*, **505**, 37–42, https://doi.org/10.1038/nature12829.

Stratton, R. A., and Coauthors, 2018: A pan-African convection-permitting regional climate simulation with the Met Office Unified Model: CP4-Africa. *J. Climate*, **31**, 3485–3508, https://doi.org/10.1175/JCLI-D-17-0503.1.

Taylor, C. M., C. E. Birch, D. J. Parker, N. Dixon, F. Guichard, G. Nikulin, and G. M. Lister, 2013: Modeling soil moisture–precipitation feedback in the Sahel: Importance of spatial scale versus convective parameterization. *Geophys. Res. Lett.*, **40**, 6213–6218, https://doi.org/10.1002/2013GL058511.

Taylor, K. E., R. J. Stouffer, and G. A. Meehl, 2012: An overview of CMIP5 and the experiment design. *Bull. Amer. Meteor. Soc.*, **93**, 485–498, https://doi.org/10.1175/BAMS-D-11-00094.1.

Tierney, J. E., C. C. Ummenhofer, and P. B. deMenocal, 2015: Past and future rainfall in the Horn of Africa. *Sci. Adv.*, **1**, e1500682, https://doi.org/10.1126/sciadv.1500682.

Tokarska, K. B., M. B. Stolpe, S. Sippel, E. M. Fischer, C. J. Smith, F. Lehner, and R. Knutti, 2020: Past warming trend constrains future warming in CMIP6 models. *Sci. Adv.*, **6**, eaaz9549, https://doi.org/10.1126/sciadv.aaz9549.

van Vuuren, D. P., and Coauthors, 2011: The representative concentration pathways: An overview. *Climatic Change*, **109**, 5–31, https://doi.org/10.1007/s10584-011-0148-z.

Vellinga, M., and S. F. Milton, 2018: Drivers of interannual variability of the East African ''long rains''. *Quart. J. Roy. Meteor. Soc.*, **144**, 861–876, https://doi.org/10.1002/qj.3263.

——, M. Roberts, P. L. Vidale, M. S. Mizielinski, M.-E. Demory, R. Schiemann, J. Strachan, and C. Bain, 2016: Sahel decadal rainfall variability and the role of model horizontal resolution. *Geophys. Res. Lett.*, **43**, 326–333, https://doi.org/10.1002/2015GL066690.

von Storch, H., and F. W. Zwiers, 1999: *Statistical Analysis in Climate Research*. Cambridge University Press, 484 pp.

Wainwright, C. M., J. H. Marsham, R. J. Keane, D. P. Rowell, D. L. Finney, E. Black, and R. P. Allan, 2019: 'Eastern African Paradox' rainfall decline due to shorter not less intense Long Rains. *npj Climate Atmos. Sci.*, **2**, 34, https://doi.org/10.1038/s41612-019-0091-7.

——, D. L. Finney, M. Kilavi, E. Black, and J. H. Marsham, 2020: Extreme rainfall in East Africa October 2019–January 2020 and context under future climate change. *Weather*, https://doi.org/10.1002/wea.3824, in press.

Walker, D. P., C. E. Birch, J. H. Marsham, A. A. Scaife, R. J. Graham, and Z. T. Segele, 2019: Skill of dynamical and GHACOF consensus seasonal forecasts of East African rainfall. *Climate Dyn.*, **53**, 4911–4935, https://doi.org/10.1007/s00382-019-04835-9.

Walters, D., and Coauthors, 2017: The Met Office Unified Model global atmosphere 6.0/6.1 and JULES global land 6.0/6.1 configurations. *Geosci. Model Dev.*, **10**, 1487–1520, https://doi.org/10.5194/gmd-10-1487-2017.

——, and Coauthors, 2019: The Met Office Unified Model Global atmosphere 7.0/7.1 and JULES global land 7.0 configurations. *Geosci. Model Dev.*, **12**, 1909–1963, https://doi.org/10.5194/gmd-12-1909-2019.

Willetts, P., J. Marsham, C. Birch, D. Parker, S. Webster, and J. Petch, 2017: Moist convection and its upscale effects in simulations of the Indian monsoon with explicit and parametrized convection. *Quart. J. Roy. Meteor. Soc.*, **143**, 1073–1085, https://doi.org/10.1002/qj.2991.

Williams, K., and Coauthors, 2015: The Met Office Global Coupled Model 2.0 (GC2) configuration. *Geosci. Model Dev.*, **8**, 1509–1524, https://doi.org/10.5194/gmd-8-1509-2015.

Woodhams, B. J., C. E. Birch, J. H. Marsham, C. L. Bain, N. M. Roberts, and D. F. Boyd, 2018: What is the added value of a convection-permitting model for forecasting extreme rainfall over tropical East Africa? *Mon. Wea. Rev.*, **146**, 2757–2780, https://doi.org/10.1175/MWR-D-17-0396.1.

Yang, W., R. Seager, M. A. Cane, and B. Lyon, 2015a: The annual cycle of East African precipitation. *J. Climate*, **28**, 2385–2404, https://doi.org/10.1175/JCLI-D-14-00484.1.

——, ——, ——, and ——, 2015b: The rainfall annual cycle bias over East Africa in CMIP5 coupled climate models. *J. Climate*, **28**, 9789–9802, https://doi.org/10.1175/JCLI-D-15-0323.1.